

Quantum-well states in metallic-thin-film overlayers

J. L. Pérez-Díaz* and M. C. Muñoz

Instituto de Ciencia de Materiales de Madrid, Consejo Superior de Investigaciones Científicas, Cantoblanco, 28049 Madrid, Spain

(Received 28 July 1995)

The electronic structure of metallic thin films grown on a semi-infinite substrate is investigated within the framework of a tight-binding model by the Green-function-matching method. An exact expression for the full Green function of the complete system is derived. It includes accurately the reduced dimensionality of the system and yields the complete description of the electronic properties: quantum-well states, resonances, and continuous substrate bands. Ag/Au(001), Co/Cu(001), and their complementary structures are selected as model systems. The calculation shows the existence of both *sp* and *d* derived quantum-well states, which are spin and symmetry dependent. The confining potential arises from the energy mismatch between thin-film overlayer and substrate bands with the same spin and symmetry. The thickness dependence of the quantum-well states' binding energy provides a mechanism to tailor the density of states at the Fermi level. [S0163-1829(96)03120-7]

I. INTRODUCTION

The electronic structure of metallic thin films grown on a substrate is very different from that of the corresponding bulk crystal. The continuous bands split up into discrete energy levels due to quantum size effects. The requirement of quantization along the film growth direction (\perp) restricts the characteristic wave vector k_{\perp} of thin-film states to specific values. This selectivity of k_{\perp} has been exploited to map three-dimensional bulk bands.¹⁻⁴ By changing the thickness of the film it is possible to determine the band dispersion relations of the overlayer material. In addition, the energy quantization has important consequences in macroscopic measurable properties of thin-film structures. In fact, reports of metallic-film quantum size effects in retarding field measurements and electron tunneling experiments go back to the earliest seventies.^{1,2} More recently, thin-film states have been directly observed by photoemission and inverse photoemission in a great variety of metallic overlayer-substrate systems.^{2,5-15} The experimental measurements show that there are two types of quantum size states: true quantum-well states (QWS's) and resonances. The former are fully confined in the film slab by an energy gap of the substrate, while resonances are bound states of the film degenerated and coupled to the continuous substrate bands. Thus, in resonances complete confinement does not happen. Although the first photoemission observations were in noble metal/semiconductor⁶ and noble metal/noble metal systems,⁵ most of the recent experimental work has been devoted to noble metal overlayers on magnetic metal substrates and to the complementary structures.⁷⁻¹⁵ The widespread interest of these systems lies on the striking properties of magnetic multilayers (ML's). They present long-range oscillatory exchange coupling¹⁶ and the change of sign in the magnetic coupling is accompanied by a giant negative magnetoresistance.¹⁷ Although several models have been proposed to explain the oscillatory nature of the exchange coupling,¹⁸⁻²² recently general consensus has been achieved and the different models can be unified into a single physical picture. The long-wavelength oscillations are produced by

polarization of *sp* valence electrons, which due to the symmetry- and spin-dependent potential discontinuities at the interfaces of an ML, are quantum-mechanically confined. This gives rise to Ruderman-Kittel-Kasuya-Yosida (RKKY) type oscillations of the exchange coupling.²³⁻²⁵ Therefore a full understanding of the coupling requires a detailed description of the ML conduction band states, which explicitly includes the reduced dimensionality and the exchange interaction. The electronic structure of thin-film overlayers on a semi-infinite substrate will display most properties of the ML electronic structure²⁶—quantum size and confinement effects. However, some discrepancies are expected due to the different characteristics of both structures. In an ML both constituent layers have finite size, while only the thin-film has finite dimension in the thin-film overlayer structure. Furthermore, the potential discontinuities at the interfaces are also different: metal-metal in ML's and vacuum-metal-metal in thin films. Most of the theoretical and experimental attention in thin-film overlayers has been focused on the existence of *sp*-like QWS's,^{7-10,14} although recently QWS's derived from *d* electrons have also been reported.^{12,13,15} On the other hand, theoretical studies rely mainly on simple models of the overlayer and substrate.^{27,28} In general, standard one-dimensional two band models are used. This restricts the calculations to the study of QWS's of a given orbital character and does not allow one to study all the QWS's derived from a band whose orbital character changes along a symmetry direction of the three-dimensional Brillouin zone.

The purpose of this work is to obtain a general description of the electronic structure of single-crystal thin-film overlayers on a semi-infinite substrate. We shall describe the bulk materials with a tight-binding (TB) model. TB Hamiltonians provide the complete band structure in which hybridization and changes of the orbital character of the bands along the symmetry directions are taken into account. The technique employed is the Green-function-matching method, which provides an exact expression for the Green function of the complete system. The approach includes explicitly the finite size of the thin film and the semi-infinite extension of the substrate. Then, the reduced dimensionality of the structure

is considered properly. Our aim is to understand the physical origin of the rich thin-film phenomenology more than to obtain quantitative agreement with experiments. The origin, orbital character, spatial confinement, and thickness dependence of both true QWS's and resonances will be investigated. We select Au/Ag(001) as a model system. Ag and Au have similar band structures in the (001) direction with the d band being well separated from the sp band. However, in spite of their similarities, energy mismatch between Ag and Au bands of the same symmetry occurs. In addition, the sign of the Ag-Au mismatch depends on the band symmetry and thus the well or barrier character of a Ag slab will change at different energy ranges. Consequently, Ag/Au(001) structures are nearly ideal for exploring quantum size and confinement effects. Furthermore, as pointed out above, magnetic structures are particularly interesting. Among them, the Cu/Co system has been widely investigated.^{7–11,13–15} Thus we will also study Cu/Co(001) structures. From the theoretical point of view, they have an added difficulty due to the spin polarization of Co electrons. Moreover, the location of the d band and the large sp - d hybridization close to E_F entangle the simple picture obtained from Ag-Au thin-film structures. Nevertheless, this complexity enriches their electronic properties. In fact, spin polarization of sp -derived QWS's, sp - d hybridization, and d -derived QWS have been reported in Co/Cu and Cu/Co thin films.^{7,8,10,11} Although there is a fairly good agreement in the experimental measurements, there are still open questions in their interpretation. To name only one among those addressed in the present study, spin-up sp QWS's for Cu/Co(001) have been reported around 1 eV below E_F , where there is not an energy gap of the substrate.^{10,11}

II. THEORY

A. Full Green function of thin-film overlayer structures

To obtain the Green function (GF) of the complete system (thin-film overlayer and semi-infinite substrate), G_S , we have used the Green-function matching method (GFMM). This approach provides a framework of exact theory in which the GF's of any layered structure can be calculated. The general formulation gives the total GF in terms of the Hamiltonian of the complete system and the bulk GF's of the constituent media. In thin-film structures with two different interfaces one matches simultaneously at the entire interface domain, which is defined as the sum of all the partial interface subdomains involved. This procedure yields a matching formula isomorphic to that for a single interface.^{28–31} Therefore we shall not derive the general expression for G_S and only the definition of the specific projection domain and the actual expressions used in the calculation will be given here.

In the particular case under study—a metallic overlayer on a semi-infinite crystal—there are two physically distinct interfaces: vacuum-overlayer and overlayer–semi-infinite crystal. Figure 1 displays the structure and notation. The overlayer and substrate crystals, denoted by A and B , respectively, have extended bulk GF G_j , $j=A,B$. Because the system retains two-dimensional (2D) periodicity, the Hamiltonian and GF are functions of the in-plane k_{\parallel} vector, energy, and spatial coordinates in the overlayer growth direction. As in previous applications of the method, we shall employ the

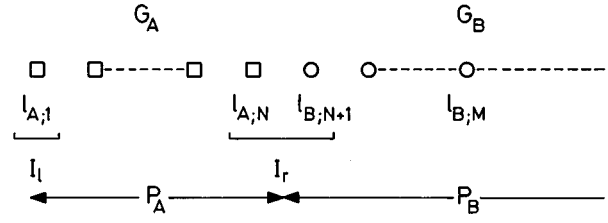


FIG. 1. Schematic representation of the thin-film overlayer structure. Each symbol depicts a principal layer. Shown are the labels used to denote the layers and the notation for the different projection domains.

concept *principal layer*, which by definition interacts only with nearest-neighbor *principal layers*. Henceforth, the k_{\parallel} and energy dependence is understood and in this subsection the term *layer* will indicate *principal layer*.

We define P_A and P_B as the unit projectors spanning the spaces of slab A and of semi-infinite B crystal, respectively. All the bulk A and B operators are only defined and evaluated in their own space. Consequently, the A interface subdomain contains two layers $l_{A;1}$ and $l_{A;N}$, while the B subdomain only holds the $l_{B;N+1}$ layer. Therefore the A and B interface projectors are $(l_{A;1}, l_{A;N})$ and $l_{B;N+1}$, respectively. The symbol $l_{j;n}$, where $j=A,B$ and n is a layer index, will be used as either the layer n of medium j or the corresponding projector.

Then the interface projection of bulk G_B is

$$\tilde{G}_B = \langle l_{B;N+1} | G_B | l_{B;N+1} \rangle = G_{B;N+1, N+1}$$

while \tilde{G}_A is a 2×2 matrix

$$\begin{aligned} \tilde{G}_A &= \begin{pmatrix} \langle l_{A;1} | G_A | l_{A;1} \rangle & \langle l_{A;1} | G_A | l_{A;N} \rangle \\ \langle l_{A;N} | G_A | l_{A;1} \rangle & \langle l_{A;N} | G_A | l_{A;N} \rangle \end{pmatrix} \\ &= \begin{pmatrix} G_{A;1,1} & G_{A;1,N} \\ G_{A;N,1} & G_{A;N,N} \end{pmatrix}. \end{aligned}$$

We define the two partial interface projectors, one for each interface: vacuum-overlayer, $I_l = l_{A;1}$, and overlayer–semi-infinite crystal, $I_r = l_{A;N} + l_{B;N+1}$. Consequently, the full interface projection is

$$I = I_l + I_r.$$

With these definitions the matching analysis yields

$$\tilde{G}_S^{-1} = IEI - IH_S P_A P_A G_A I_A \tilde{G}_A^{-1} - IH_S P_B P_B G_B I_B \tilde{G}_B^{-1}. \quad (1)$$

This formula cannot be read as ordinary algebraic expressions. Instead, all the operations, including inversion, must be performed always within the space in which objects are defined.

After some algebra and using the relations between Green functions and transfer matrices T, \bar{T}, S, \bar{S} :

$$G_{n+1,m} = T G_{n,m}, \quad n \geq m, \quad (2)$$

$$G_{n-1,m} = \bar{T}G_{n,m}, \quad n \leq m,$$

$$G_{n,m-1} = G_{n,m}\bar{S}, \quad n \geq m.$$

$$G_{n,m+1} = G_{n,m}S, \quad n \leq m,$$

Equation (1) can be cast as a 3×3 supermatrix:

$$\tilde{G}_S^{-1} = \begin{pmatrix} E - H_{A;1,1} - D_{A;1,1} & -D_{A;1,N} & 0 \\ -D_{A;N,1} & E - H_{A;N,N} - D_{A;N,N} & -H_{AB;N,N+1} \\ 0 & -H_{BA;N+1,N} & E - H_{B;N+1,N+1} - D_{B;N+1,N+1} \end{pmatrix} \quad (3)$$

where

$$\begin{aligned} D_A &= \begin{pmatrix} D_{A;1,1} & D_{A;1,N} \\ D_{A;N,1} & D_{A;N,N} \end{pmatrix} \\ &= \begin{pmatrix} H_{A;1,2} & 0 \\ 0 & H_{A;N,N+1} \end{pmatrix} \begin{pmatrix} T_A & \bar{T}_A^{N-2} \\ T_A^{N-2} & \bar{T}_A \end{pmatrix} \begin{pmatrix} 1 & \bar{T}_A^{N-1} \\ T_A^{N-1} & 1 \end{pmatrix}^{-1} \end{aligned}$$

and

$$D_B = H_{B;N+1,N+2}T_B.$$

T_j and \bar{T}_j ($j=A,B$) are the transfer matrices introduced in Eq. (2), $H_{j;n,m}$ ($j=A,B$) the Hamiltonian matrix element between layers n and m , and $H_{AB;n,m}$ the coupling interaction across the overlayer–semi-infinite crystal interface.

Expression (3) for \tilde{G}_S^{-1} is particularly suitable for actual calculation since it avoids the cumbersome integration required to calculate diagonal and nondiagonal elements of the bulk GF G_j ($j=A,B$).

From \tilde{G}_S , the matrix elements of G_S between any layers of the entire structure are obtained from

$$G_{S;n,m} = \begin{cases} G_{A;n,m} + (G_{A;n,1}, G_{A;n,N}) \tilde{G}_A^{-1} (\tilde{G}_S - \tilde{G}_A) \tilde{G}_A^{-1} \begin{pmatrix} G_{A;1,m} \\ G_{A;N,m} \end{pmatrix}, & n, m \in A \\ (G_{A;n,1}, G_{A;n,N}) \tilde{G}_A^{-1} \tilde{G}_S \tilde{G}_B^{-1} G_{B;N,m}, & n \in A, m \in B \\ G_{B;n,N} \tilde{G}_B^{-1} \tilde{G}_S \tilde{G}_A^{-1} \begin{pmatrix} G_{A;1,m} \\ G_{A;N,m} \end{pmatrix}, & n \in B, m \in A \\ G_{B;n,m} + G_{B;n,N} \tilde{G}_B^{-1} (\tilde{G}_S - \tilde{G}_B) \tilde{G}_B^{-1} G_{B;N,m}, & n, m \in B. \end{cases} \quad (4)$$

In particular, the diagonal matrix elements of G_S are

$$G_{S;n,n} = \begin{cases} G_{A;n,n} + (T_A^{n-1}, \bar{T}_A^{N-n}) \begin{pmatrix} 1 & \bar{T}_A^{N-1} \\ T_A^{N-1} & 1 \end{pmatrix}^{-1} (\tilde{G}_S - \tilde{G}_A) \begin{pmatrix} 1 & S_A^{N-1} \\ \bar{S}_A^{N-1} & 1 \end{pmatrix}^{-1} \begin{pmatrix} S_A^{n-1} \\ \bar{S}_A^{N-n} \end{pmatrix}, & n \in A \\ G_{B;n,n} + T_B^{n-N-1} (\tilde{G}_S - \tilde{G}_B) S_B^{n-N-1}, & n \in B \end{cases} \quad (5)$$

and the layer density of states (LDOS) in any layer is given by

$$N_n(k_{\parallel}, E) = -\frac{1}{\pi} \lim_{\epsilon \rightarrow 0} \text{Im} \text{Tr} G_{S;n,n}(k_{\parallel}, E + i\epsilon). \quad (6)$$

Although the derivation of G_S is exact, the accuracy of actual calculations depend on the Hamiltonian model. Thus, in the present calculation it is determined by the accuracy of the TB parameters.

B. Hamiltonian model

The empirical tight-binding (ETB) Hamiltonians of Papaconstantopoulos³² have been used to describe the Au,

Ag, Cu, and paramagnetic fcc Co bulk materials. They take into account second-nearest-neighbor interactions and the *spd* orbital basis set. The ferromagnetic Co Hamiltonian includes a diagonal band-dependent exchange interaction. The calculation of the exchange contribution to the ferromagnetic matrix elements was performed by fitting the self-consistent spin-polarized Korringa-Kohn-Rostoker (KKR) band structure of Moruzzi, Janak, and Williams³³ and available experiment data in the ΓX direction.^{7,34} The exchange interactions are $\Delta_s = 0.088$, $\Delta_p = 0.054$, $\Delta_{d-t_{2g}} = 0.832$, and $\Delta_{d-e_g} = 0.849$ eV. The resulting Co ETB Hamiltonian describes quite accurately the dispersion relations in the high energy region close to E_F , although it gives a poorer de-

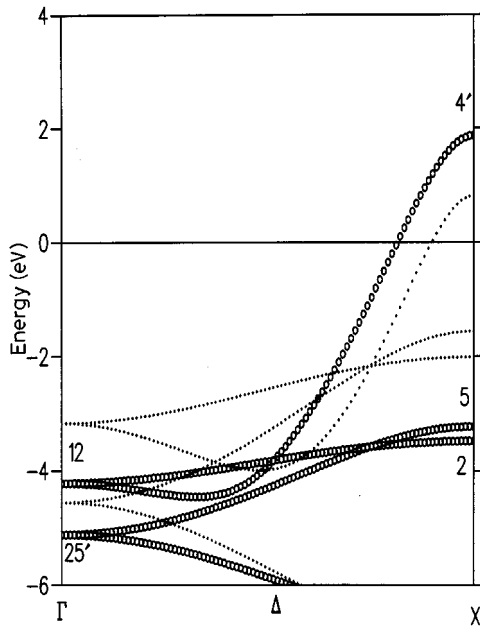


FIG. 2. Energy bands of Ag and Au along the ΓX direction, from -6 to 4 eV above the Fermi level. The energies in eV are relative to the Fermi energy. Open circles and dots represent Ag and Au states, respectively.

scription of the X_1 and X_3 band splitting. The calculated magnetic moment per atom is $1.56\mu_B$. For the cross coupling matrix elements at the interfaces we have taken the arithmetic average of the corresponding bulk parameters. These values yield zero net charge for the semi-infinite interfaces.³⁵ Furthermore, in the Co/Cu(001) interface, the average d -interface potentials result in interface spin polarization and magnetic moments whose sign and magnitude agree with those recently measured.³⁶ The surface Hamiltonian matrix elements are kept equal to those of bulk. In the spin-polarized calculation of the Co(100) surface, charge neutrality was attained in the entire semicrystal with zero surface potential. However, in the Cu(001) surface, the self-consistent surface potential is less attractive than the corresponding bulk potential for d electrons.³⁵ Then, due to its Tamm character, the Cu(001) d -like surface states at \bar{M} will not be properly described in our calculation. In summary, the use of bulk TB parameters at surfaces and average values at interfaces is expected to slightly alter the energy position of Cu QWS's only for Cu thin-film grown on Co semicrystals. We consider ideal structures grown in the fcc (001) direction with matched overlayer and substrate lattice parameters.

III. NOBLE METAL OVERLAYERS: Ag AND Au (001)

Silver and gold are noble metals with similar electronic band structures. In both, the Fermi level E_F intersects the sp band at points where it resembles a free electron-like band and further down lies the complex d band. The Ag d bands are narrower and located deeper than those of Au. Figure 2 shows the dispersion relation of the bulk bands along the ΓX direction for an energy window of 10 eV around E_F . In the whole energy interval the Au d bands stay above those of Ag. Nevertheless, depending on the band

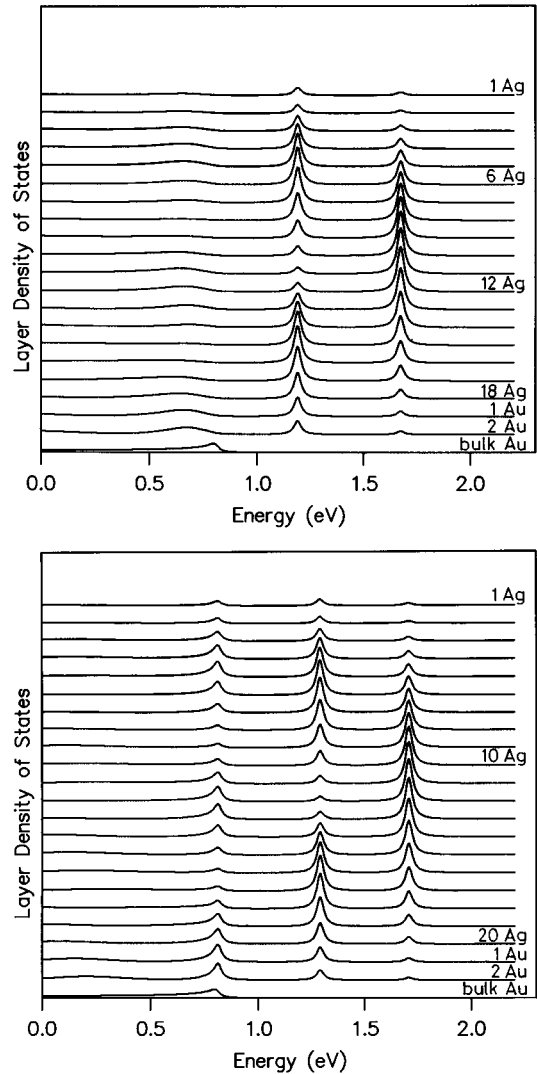


FIG. 3. sp component of the layer density of states at the $\bar{\Gamma}$ point of the 2D Brillouin zone for 18 (upper panel) and 20 (lower panel) ml of Ag on Au(001). From top to bottom the LDOS for the Ag, two Au, and a bulk Au layer of the semi-infinite crystal are represented.

symmetry, their (001) projections may or may not overlap. For instance, the bottom of the Au Δ_2 band, the Γ_{12} level, is above the Ag X_2 top edge. Therefore, Δ_2 Au and Ag bands do not overlap. In contrast, the Δ_5 bands overlap for energies below the Ag X_5 edge. On the other hand, the Δ_1 Au band, in the energy region with a predominantly sp character, is always beneath the corresponding Δ_1 Ag band and, except for an energy window of 1 eV above the $X_{4'}$ Au edge, Δ_1 Au and Ag bands overlap. It is in the energy intervals in which the projected bands do not overlap that one expects to find quantized discrete states—so called QWS's. Figure 3 displays the sp -like component of the LDOS at $\bar{\Gamma}$ obtained for 18 and 20 monolayers (ml) of Ag on Au(001). In the energy interval shown in the figure, the d -like contribution to the LDOS is negligible. For the 18 ml film there are two well defined states above the Au $X_{4'}$ edge, labeled $n=1$ and $n=2$ at 1.7 and 1.2 eV, respectively. Furthermore, below the $X_{4'}$ Au level—around 0.65 eV—a smooth modulation of the Ag LDOS is also noticeable. As the Ag film thickness in-

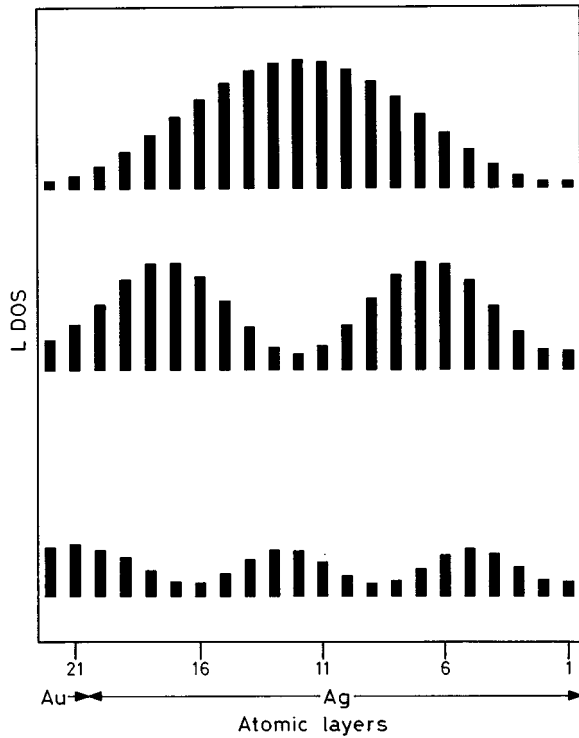


FIG. 4. Local spectral strength of the three QWS's at the $\bar{\Gamma}$ point for the 20 ml Ag thin film. The figure displays the spatial distribution in the different atomic layers of the structure.

creases to 20 ml, this broad structure moves just above the Au $X_{4'}$ edge and becomes a well defined $n=3$ peak. The other two states also move upwards in energy. Figure 4 represents the squared amplitude of the corresponding wave functions for the 20 ml Ag film. All the states are localized in the Ag overlayer, although the amplitudes spread out increasingly from the Ag film as the order of the state increases. For instance, the lowest level, $n=3$ penetrates quite considerably, as it corresponds to a less tightly bound state. Their spatial distribution presents one, two, and three maxima for $n=1$, $n=2$, and $n=3$, respectively. In addition, the amplitude is larger at the interface Ag layer than at the surface, due to the lower height of the interface barrier. Figure 5 shows the energy of the discrete states versus the number of Ag ml's. With increasing Ag thickness more states appear above the Au $X_{4'}$ edge and continuously move upwards towards the Ag $X_{4'}$ level. Consequently, the observed structures are identified as sp -like size-quantized states of the Ag slab, whose characteristic wave vector normal to the layer is restricted by the size-quantization condition to $\pm k_{\perp}$ where

$$k_{\perp} = \frac{n\pi}{(N+1)d}, \quad n=1, \dots, N. \quad (7)$$

N is the number of layers and d the interlayer spacing. The confining QW structure is due to the Ag and Au Δ_1 band mismatch at the $X_{4'}$ edge. The Ag slab acts as a QW, the Au substrate being a barrier. In first order, the energy of the QWS's can be obtained directly from the Ag bulk dispersion relation $E=E(k_{\perp})$ and the size-quantization condition (7).

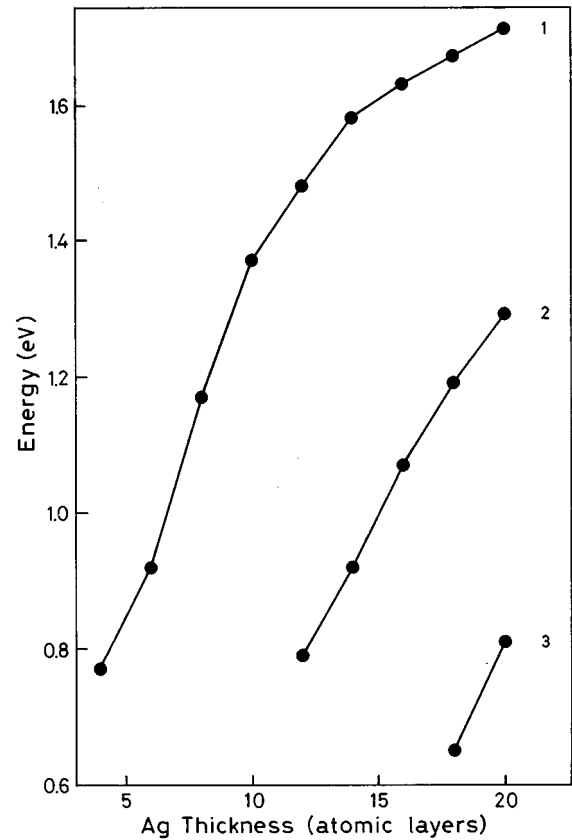


FIG. 5. Binding energy of the sp -derived Ag QWS's as a function of the Ag film thickness. The numbers at right label the quantum-well numbers.

Therefore the QW energy spectra of an N -layer thick slab correspond to those bulk levels which result from sampling the band at N equidistant k points. In fact, accurate bulk band structure information has been obtained from thin-film structures.³ However, due to the finite Au-Ag and surface barrier heights, a small energy difference between bulk and QWS's for a given k_{\perp} is expected. Furthermore, at a fixed energy E , a size-quantized state will appear periodically with the slab thickness. That is, there will be a new state whenever k_{\perp} satisfies the quantization condition (7). Consequently, at a given energy, there is a simple relation between the period $L(E)$ and the size-quantized state wave vector $k_{\perp}(E)$:

$$L(E) = \frac{\pi}{|k_{\perp}(E) - k_{ZB}|d} \quad (8)$$

where k_{ZB} is the zone boundary wave vector. For the data shown in Fig. 5, $k_{ZB}=X_{4'}$ and $L(X_{4'}) \approx 8$ ml. When the energies of the states satisfying Eq. (7) are in a forbidden substrate gap— $n=1$ and $n=2$ peaks in Fig. 3—they are well defined bound QWS's mostly confined in the Ag slab. Moreover, for the unbounded motion, i.e., states whose energy is allowed for the substrate, size-quantization effects also manifest themselves as Ag film resonances. See the structure at -0.65 eV in Fig. 3.

As remarked previously, in the energy interval from -2 to -6 eV the Au d bands are above the corresponding Ag

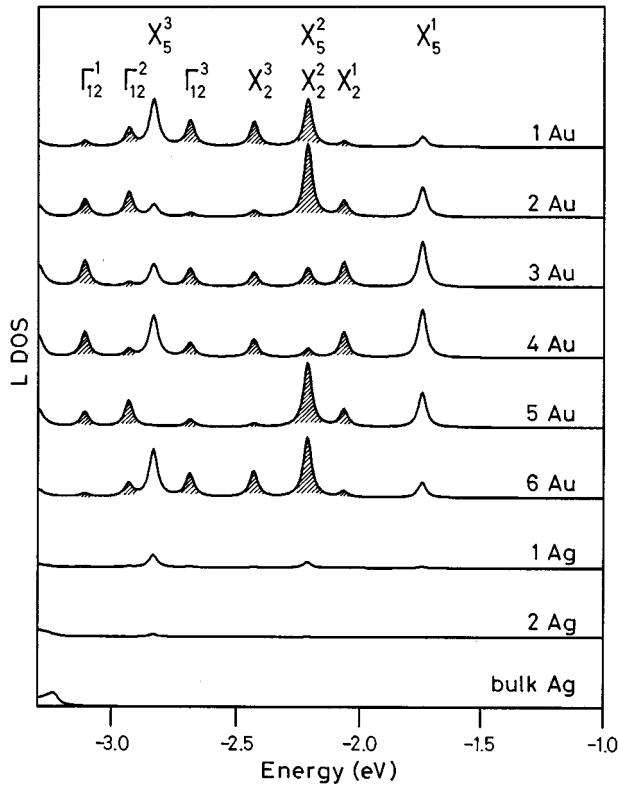


FIG. 6. d component of the layer density of states at the $\bar{\Gamma}$ point of the 2D Brillouin zone for 6 ml of Au on Ag(001). As in Fig. 3 the LDOS's for the Au, two Ag, and a bulk Ag layer are represented. The peaks are labeled by the bulk energy level of origin and superscripts indicate quantum-well number (see text). The QWS's derived from the Δ_2 Ag band are dashed.

ones. Moreover, bands of the same symmetry do not overlap, either in the complete band energy range, Δ_2 , or in an appreciable region, Δ_5 close to the X_5 border and Δ_1 close to Γ_{12} . Therefore, Au overlayers on Ag(001), will present d -derived Au QWS's in these energy intervals. Note that the previously described sp -like QWS's appear in the complementary Ag/Au (001) structure. Figure 6 displays the d -component LDOS for 6 ml of Au on a semi-infinite (001) Ag crystal. Similarly to the sp -like LDOS of Fig. 3, well defined d -like QWS's are clearly observed. Furthermore, there is almost complete confinement of states. Only two states present a very small amplitude at the first Ag layer. However, the states do not show $n=1,2,3,\dots$ maxima in a sequential order; instead, crossing of various QWS series takes place. A detailed analysis of the QWS wave-function spatial and orbital symmetry and their evolution with the number of Au layers allows one to identify three series of d -like QWS's. They originate from Au bands of different symmetry and are associated with the Au-Ag mismatch of the X_5 , X_2 , and Γ_{12} levels. Henceforth, we label the QWS's series by the energy level of origin. Figure 7, which represents the squared amplitude of the four highest energy states, evidences the crossing of QWS series. From top to bottom there are two $n=1$ QWS's of the X_5 and X_2 series, respectively, an $n=2$, and the $n=3$ of X_2 . In the third state, $n=2$, the displayed LDOS is in fact the sum of the second-

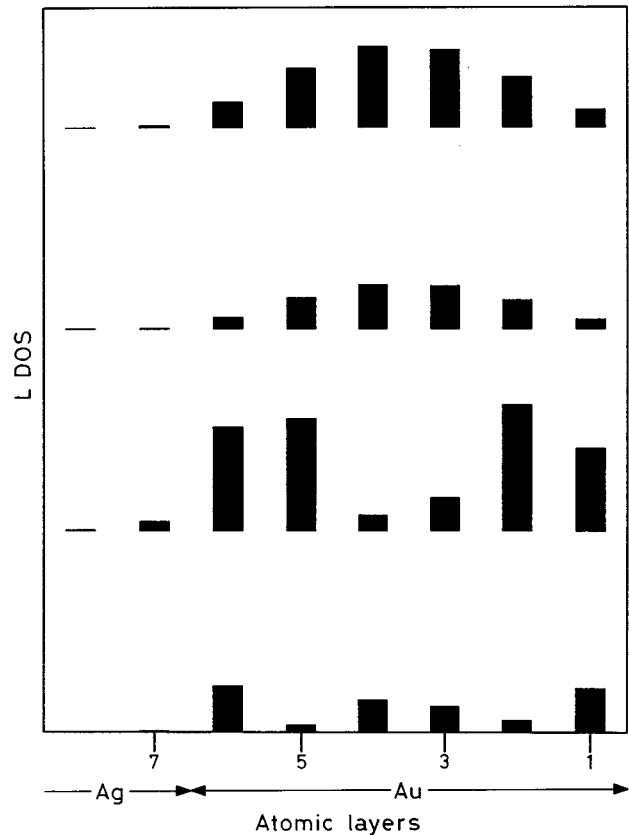


FIG. 7. Local spectral strength of the four highest energy QWS's of Fig. 6. The figure displays the spatial distribution in the Au and in the two first Ag layers.

order states of both X_5 and X_2 series, which become almost degenerate in energy. In addition, because of the heaviest effective mass of d electrons, a large number of QWS's appears in an energy interval for small overlayer thicknesses—see Fig. 6. Consequently, the density of QWS's is proportional to the effective mass of the corresponding bulk band, and dispersionless bands tend to form densely spaced QWS's. Figure 8 represents the energy of the d -like QWS's as a function of the slab thicknesses. The evolution of the three series identified in Fig. 6 is presented. For a given number of Au ml, the lower density of X_5 QWS's shows the higher dispersion of the Δ_5 band with respect to Δ_2 . Nevertheless, the more important point shown by Fig. 8 is that each band, Δ_2 in the figure, generates two series of QWS's. With increasing overlayer thickness each series moves in energy towards a band extreme. Positive/negative effective mass at the zone boundary gives rise to QWS series whose states move downward/upward in energy. Furthermore, since the entire Δ_2 Au band does not overlap with the corresponding Ag one, the whole Δ_2 Au is quantized and the number of QWS's is equal to the number of layers. This is exemplified in Fig. 6, where the states coming from the Δ_2 band are dashed (there are three associated with Γ_{12} and three with X_2).

IV. SPIN-POLARIZED QW'S: Cu AND Co (001)

The Cu electronic structure, with filled d bands and a partially occupied sp band, is similar to those of Ag and Au

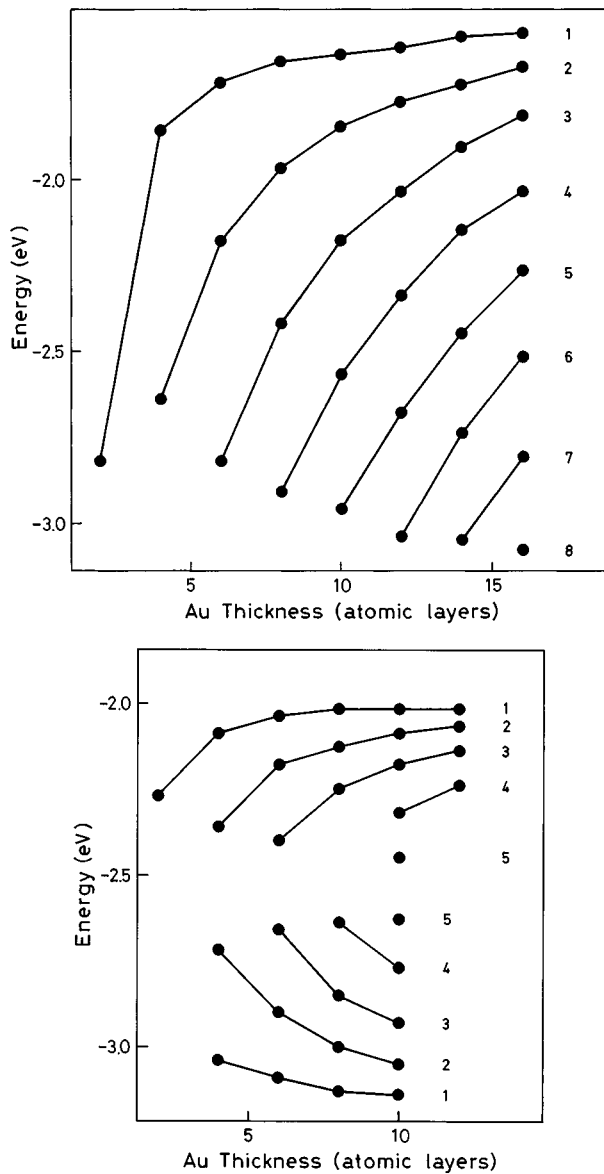


FIG. 8. Binding energy of d -derived Au QWS's as a function of the Au slab thickness. The evolution of the X_5 QWS's series is presented in the top panel, and that of X_2 and Γ_{12} series at the bottom. As in Fig. 5 the quantum-well numbers are indicated at the right of the curves.

previously described. However, in the case of Co, the exchange interaction gives rise to an exchange splitting of majority (\uparrow) and minority (\downarrow) spin bands. The Fermi level lies within the minority d band, while the majority band stays just below E_F . Figure 9 presents the Co and Cu band structures along the ΓX direction in an energy interval close to E_F . Due to the Co exchange splitting and to the difference between Co and Cu d -band widths, the relative alignment of Co and Cu bands of the same symmetry is spin dependent and the well or barrier character of the overlayer slab may be different for both spins. For example, while the majority-spin $\Delta_{2'}$ Co band intersects the corresponding $\Delta_{2'}$ of Cu, the minority $\Delta_{2'}$ is always above that of Cu. Therefore Co overlayers should present two series of spin-up $\Delta_{2'}$ QWS's associated with $\Gamma_{25'}$ and X_3 , and only one associated with $\Gamma_{25'}$ for spin-down electrons. The rich phenomenology of

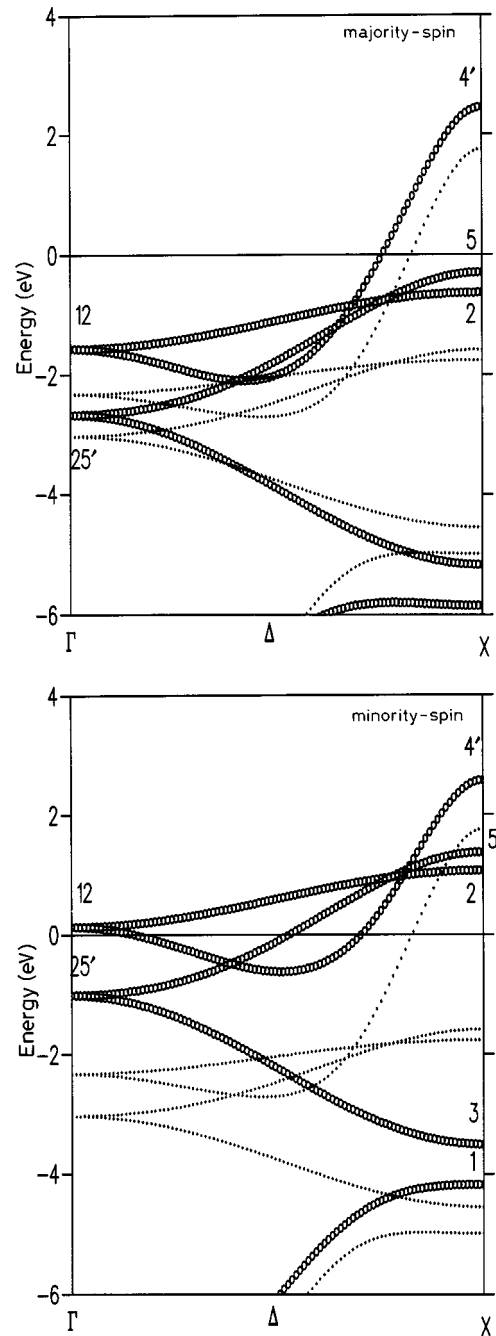


FIG. 9. Energy bands of Cu and ferromagnetic fcc Co along the ΓX direction for an energy interval of 10 eV around E_F . The energies in eV are referred to the Fermi level. Open circles and dots represent Co and Cu bands, respectively. Majority-spin states are displayed at the top and minority-spin states at the bottom.

magnetic structures is clearly illustrated in Figs. 10 and 11 where the spin-polarized d -like contributions to the LDOS around the X_1 and X_3 bulk levels are shown for 6 ml of Cu on Co(001) and 6 ml of Co on Cu(001). In the Cu overlayer system X_1 , $n=1$ and $n=2$, Cu QWS's appear above the Co X_1 level for spin-up electrons [Fig. 10 (top panel)], while spin-down X_3 QWS's from $n=1$ to $n=4$ are clearly seen in the minority LDOS [Fig. 10 (bottom panel)]. The larger level density of minority X_3 QWS's is due to the higher effective mass—lower curvature—of the X_3 Cu band. Furthermore, in the majority LDOS the formation of the X_3 Cu border and

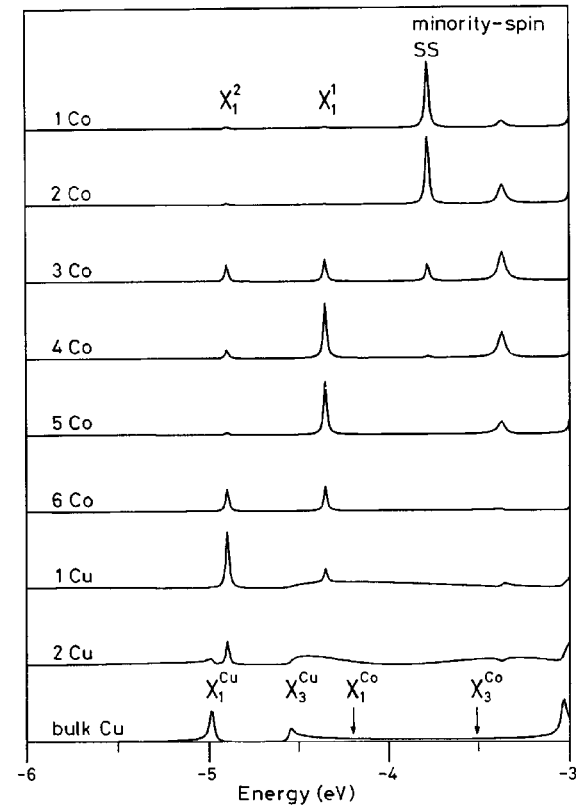
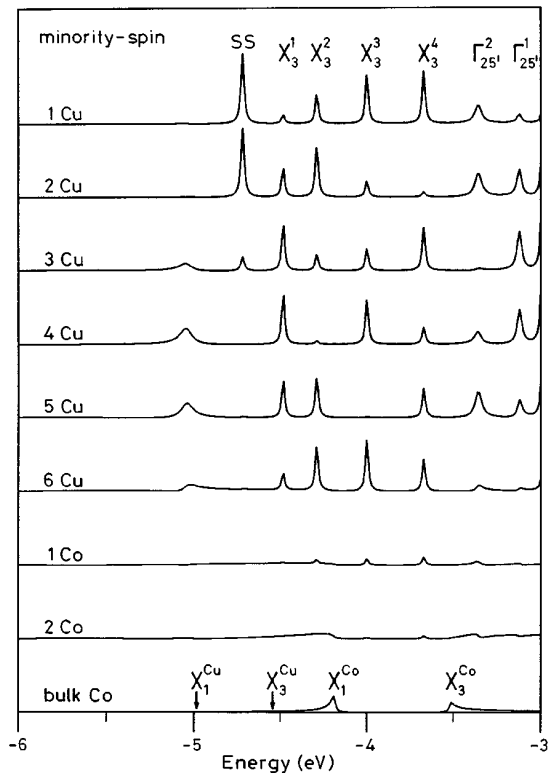
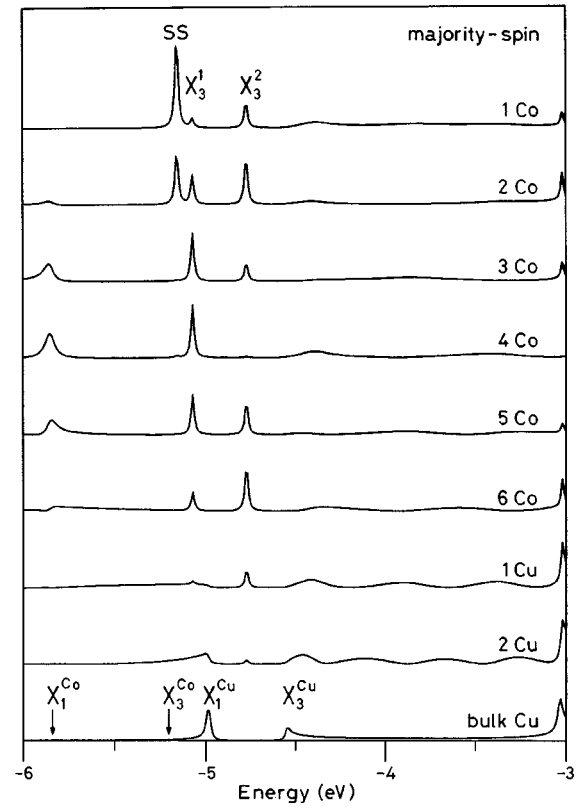
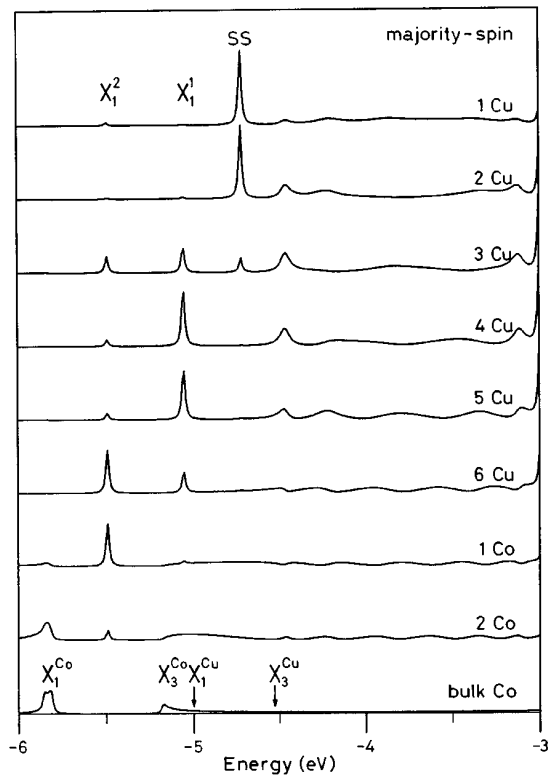


FIG. 10. d component of the layer density of states at the $\bar{\Gamma}$ point of the 2D Brillouin zone for 6 ml of Cu on Co (001) around the X_1 and X_3 bulk levels. The LDOS's for the thin film, two interface, and a bulk substrate layer are represented. An arrow indicates the position of the overlayer X_1 and X_3 bulk levels. Majority- and minority-spin LDOS's are displayed at top and bottom, respectively.

FIG. 11. Same as Fig. 10 for 6 ml of Co on Cu(001). associated Cu resonances is clearly seen for energies above -4.5 eV. In addition to the X_3 QWS's series, $n=1$ and $n=2$ Δ_5 QWS's associated with the $\Gamma_{25'}$ border also appear in the minority LDOS at high energies. The squared amplitude of all the peaks behaves as corresponds to well defined

QWS's. On the other hand, in the 6-ml Co/Cu(001) structure (see Fig. 11) the role of majority and minority spins interchanges. Now, the majority LDOS presents X_3 $n=1$ and $n=2$ QWS's while the X_1 series develops for minority spin electrons. The results are easily understood by inspection of Fig. 9. At X the Co slab behaves as a well/barrier for Δ_2 , majority/minority electrons and contrarily for Δ_1 . Therefore Co slabs act as a well or as a barrier for electrons with the same symmetry but different spin polarization and as a consequence QWS's are spin polarized, even those derived from Cu electrons. Furthermore, all the spectra of Figs. 10 and 11 show states well localized in the outermost slab layers. They are *bona fide* surface states which become noticeable for overlayers 2 ml thick. Their energies are thickness independent and are those found in surfaces of semi-infinite crystals. They are located at the energy gaps of the bulk projected band structure. See Figs. 3 and 4 of Ref. 35. Similar effects occur for truly interface states—developed in mutual gaps of both semi-infinite crystals. However, if the state associated with the surface or interface is a resonance, its thickness dependence is quite different. They are only noticeable as an enhancement of the interface LDOS of a QWS's peak. Notice the state located at -5.5 eV in the majority LDOS for 6 ml Cu on Co (Fig. 10). In the semi-infinite Co/Cu interface also an interface resonance is found at -5.5 eV.³⁵ The spatial distribution of the amplitude of this structure corresponds to an $n=2$ QWS; however, the intensity of the interface layers has increased considerably. Thus, while interface resonances have to satisfy the size-quantization condition, truly interface states, developed in mutual gaps, do not. As explained above, E_F lies within the minority Co d bands, which are above those of Cu. Therefore Co/Cu(001) will present a large density of minority-spin QWS's in the energy interval around E_F . Furthermore, because of the size-quantization condition, the energy of QWS's is thickness dependent. Thus, selecting the overlayer thickness, one can find a QWS in a given small energy interval, particularly close to the Fermi level. This fact is exemplified in Fig. 12 which displays the minority LDOS around E_F for 6 ml of Co on Cu(001). Therefore, the LDOS at the Fermi level can be controlled by regulating the overlayer thickness. Since many macroscopic physical properties depend on the LDOS at the Fermi level, overlayer thickness selection provides a mechanism to tailor macroscopic properties of thin-film overlayers. In addition to the Δ_1 QWS at E_F , in the energy interval shown in Fig. 12, there is a great concentration of QWS's arising from quantization of Δ_5 and Δ_2 bands. For the sake of clarity only states with Δ_2 symmetry are marked. This band does not overlap with Δ_2 of Cu and is completely quantized, similarly to the Δ_2 band in Au/Ag(001)—see Fig. 6.

In the Co/Cu system sp -derived QWS's have been identified in unresolved and spin-resolved photoemission spectra. The Δ_1 Cu and Co bands have mainly sp character from approximately the middle of the ΓX direction to the X boundary. Therefore, sp QWS's and resonances can develop in the energy interval $\delta E = E_{Co}(X_{4'}) - E_{Cu}(k \approx \pi/2d)$, that is, from -3.0 to 2.5 eV. Above the Fermi level, the exchange splitting of the majority and minority Δ_1 bands is small. The effective mass is negative and the Co bands for both spins have higher energy than those of Cu. Therefore Co overlayers on Cu(001) show

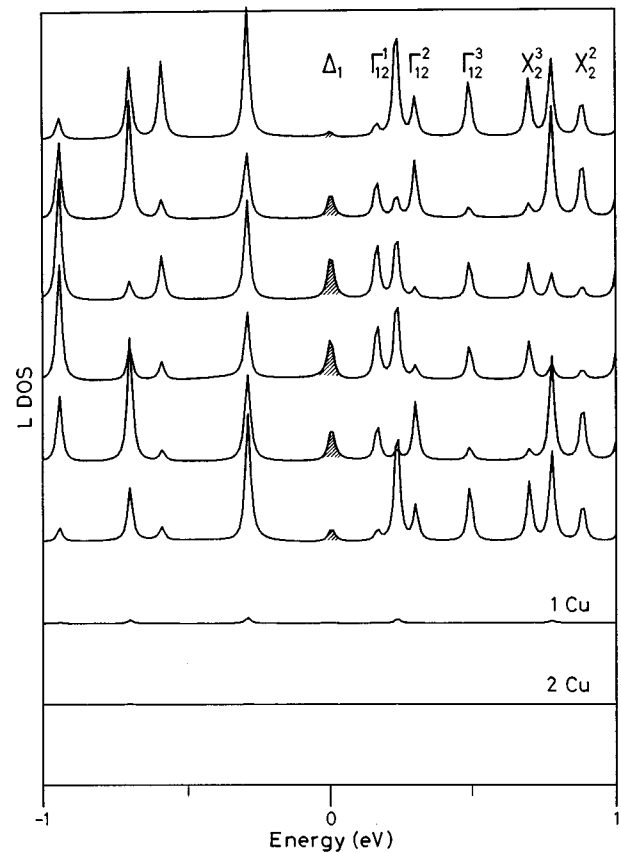


FIG. 12. Minority-spin d component of the LDOS at $\bar{\Gamma}$ for 6 ml of Co on Cu(001) around E_F . The Δ_1 QWS's at E_F is dashed.

sp -like Co QWS's above the X_4 Cu level. The energy splitting between majority and minority QWS's is small. The behavior of these states is analogous to that of sp -like Ag QWS's shown in Fig. 5 and previously described. These states have been experimentally observed by unresolved inverse photoemission (Fig. 2 of Ref. 9). Below E_F the Δ_1 band curvature changes sign and the Co band remains above the Cu—see Fig. 2. Therefore QWS's will develop only in Cu overlayers. Furthermore, at these energies, the Δ_1 Co band has a large splitting, which results in very different majority and minority Co-Cu energy gaps. Consequently, the sp -derived QWS's close to E_F will be spin polarized. This explains the different behavior of majority and minority electrons experimentally observed in spin-resolved photoemission experiments.^{10,11} Moreover, in this energy range there is overlap with the d bands. Therefore strong sp - d hybridization is expected. Figure 13 shows the LDOS of the outermost Cu layer in 2 ml Cu/Co(001). The LDOS is orbital and spin resolved. The majority sp -like LDOS does not present any pure sp -like QWS's in this energy interval; the two peaks seen at low energy have a mainly d character and reflect the strong sp - d hybridization of the Cu bands. Note the different scale of the sp and d LDOS's. Thus, although the Cu/Co gap is very small for majority electrons, sp - d hybridization promotes the formation of QWS's. On the other hand, the minority sp -like LDOS shows a well defined QWS's around -1 eV, although it also has an important d contribution. These findings agree with the experimental observations of

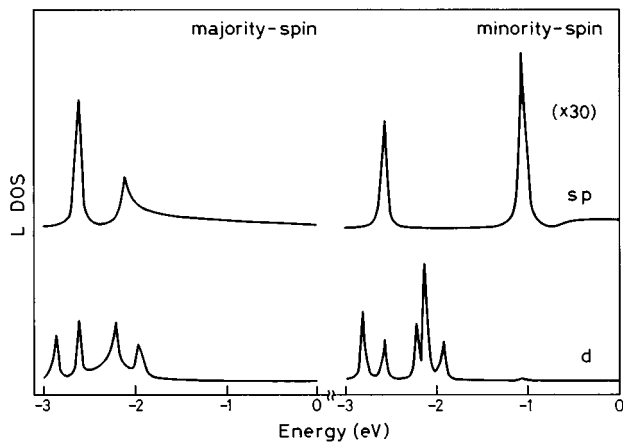


FIG. 13. Orbital- and spin-resolved LDOS at $\bar{\Gamma}$ of the outermost Cu layer for 2 ml Cu film on Co(001). *sp* and *d* components of the LDOS are displayed at top and bottom, respectively.

sp polarization and *sp-d* hybridization in Cu/Co(001) overlayers.^{10,11} Thus the spin polarization of Cu-derived QWS's manifests the different energy gap of the majority and minority substrate Co bands. Furthermore, all the experimentally measured peaks in this energy range are hybrid states with both *sp* and *d* orbital components.

V. CONCLUDING REMARKS

The electronic structure of metallic-thin-film overlayers grown on a substrate can be fully described in terms of the overlayer size-quantized states and continuous substrate bands. The wave-vector component in the growth direction, k_{\perp} , of thin-film states is quantized due to its finite thickness. There are two types of bound states: QWS's and resonances. The former are fully confined by an energy gap of the sub-

strate while the second are extended and degenerate with the continuous substrate band. Both QWS's and resonances show spatial modulation of the wave-function amplitude and the number of maxima corresponds to the order of the bound state. Their binding energy is film-thickness dependent and a quantum-well picture based on the quantization of bulklike bands of a given symmetry describes their development. The well or barrier character of the thin film depends on the relative alignment of overlayers and substrate bands of the same symmetry. Furthermore, the thickness dependence of the QWS binding energy provides a mechanism to control the density of states at the Fermi level and, as a consequence, metallic-thin-film overlayer structures can be grown with tailored macroscopic properties.

The Ag/Au(001) and Co/Cu(001) structures, as well as the complementary systems, support both *sp*- and *d*-like QWS's. Since the *d*-bands are narrow, there is a large density of *d*-derived QWS's. Thus, experimental observation of *d*-like QWS's demands very high energy resolution. In the Co/Cu system QWS's are spin dependent due to the large exchange splitting of Co *d* bands. The QWS's observed close to E_F in Cu films grown on Co(001) are spin polarized due to *sp-d* hybridization. In summary, a proper analysis of size-quantized states in thin-film overlayers requires a complete description of the bulk bands of both overlayers and substrate crystals. The electronic properties of thin films are determined by both size-quantization and confinement effects. Band symmetry, relative alignment of overlayer and substrate bands, spin, and hybridization combine to settle their actual structure.

ACKNOWLEDGMENTS

This work was supported by the Spanish Dirección General de Investigación Científica y Técnica under Grant No PB93-1252.

*Permanent address: Escuela Politecnica Superior, Universidad Carlos III de Madrid, Butarque 15, 28911 Leganes, Spain.

¹R.E. Thomas, J. Appl. Phys. **41**, 5330 (1970).

²R.C. Jacklevic, J. Lambe, M. Mikko, and W.C. Vassell, Phys. Rev. Lett. **26**, 88 (1971); R.C. Jacklevic and J. Lambe, Phys. Rev. B **12**, 4146 (1975).

³M.A. Mueller, T. Miller, and T.-C. Chiang, Phys. Rev. B **41**, 5214 (1990).

⁴F.J. Himpsel, Phys. Rev. B **44**, 5966 (1991).

⁵T. Miller, A. Samsavar, G.E. Franklin, and T.-C. Chiang, Phys. Rev. Lett. **61**, 1404 (1988).

⁶A.L. Wachs, A.P. Shapiro, T.C. Hsieh, and T.-C. Chiang, Phys. Rev. B **33**, 1460 (1986).

⁷W. Clemens, T. Kachel, O. Rader, E. Vescovo, S. Blügel, C. Carbone, and W. Eberhardt, Solid State Commun. **81**, 739 (1992).

⁸J.E. Ortega and F.J. Himpsel, Phys. Rev. Lett. **69**, 844 (1992).

⁹J.E. Ortega, F.J. Himpsel, G.J. Mankey, and R.F. Willis, Phys. Rev. B **47**, 1540 (1993).

¹⁰K. Garrison, Y. Chang, and P.D. Johnson, Phys. Rev. Lett. **71**, 2801 (1993).

¹¹C. Carbone, E. Vescovo, O. Rader, W. Gudat, and W. Eberhardt, Phys. Rev. Lett. **71**, 2805 (1993).

¹²D. Hartmann, W. Weber, A. Rampe, S. Popovic, and G. Güntherodt, Phys. Rev. B **48**, 16 837 (1993).

¹³G.J. Mankey, R.F. Willis, J.E. Ortega, and F.J. Himpsel, J. Vac. Sci. Technol. A **12**, 2183 (1994).

¹⁴C. Carbone, E. Vescovo, R. Kildsges, W. Eberhardt, O. Rader, and W. Gudat, J. Appl. Phys. **76**, 6966 (1994).

¹⁵P.D. Johnson, K. Garrison, Q. Dong, N.V. Smith, D. Li, J. Mattson, J. Pearson, and S.D. Bader, Phys. Rev. B **50**, 8954 (1994).

¹⁶S.S.P. Parkin, R. Bhadra, and K.P. Roche, Phys. Rev. Lett. **66**, 2152 (1991); S.S.P. Parkin, *ibid.* **67**, 3598 (1991); B. Heinrich, Z. Celinski, K. Myrtle, J.F. Cochran, M. Kowalewski, A.S. Arrott, and J. Kirschner, J. Appl. Phys. **69**, 5217 (1991); F. Petroff, A. Barthélemy, D.H. Mosca, D.K. Lottis, A. Fert, P.A. Schroeder, W.P. Pratt, Jr., R. Loloee, and S. Lequien, Phys. Rev. B **44**, 5355 (1991); C.M. Schneider, P. Bressler, P. Schuster, J. Kirschner, J.J. de Miguel, and R. Miranda, *ibid.* **64**, 1059 (1990); W. R. Bennett, W. Schwarzacher, and W.F. Egelhoff, Phys. Rev. Lett. **65**, 3169 (1990), and references therein.

¹⁷S.S.P. Parkin, N. More, and K. P. Roche, Phys. Rev. Lett. **64**, 2304 (1990); P. Grünberg, R. Schreiber, Y. Pang, M.B. Brodsky, and H. Sowers, *ibid.* **57**, 2442 (1986); P. Eitenne, J. Chazelas, G. Cruezet, A. Frederick, and J. Massies, J. Cryst. Growth **95**, 410 (1989); M.N. Baibich, J.M. Broto, A. Fert, F. Nguyen Van Dau,

- F. Petroff, P. Eitenne, G. Creuzet, A. Friederich, and J. Chazelas, *Phys. Rev. Lett.* **61**, 2472 (1988); G. Binasch, P. Grünberg, F. Saurenbach, and W. Zinn, *Phys. Rev. B* **39**, 4828 (1989).
- ¹⁸P. Bruno and C. Chappert, *Phys. Rev. Lett.* **67**, 1602 (1991).
- ¹⁹D.M. Edwards, J. Mathon, R.B. Muniz, and M.S. Phan, *Phys. Rev. Lett.* **67**, 493 (1991).
- ²⁰M.D. Stiles, *Phys. Rev. B* **48**, 7238 (1993).
- ²¹M.C. Muñoz and J.L. Pérez-Díaz, *Phys. Rev. Lett.* **72**, 2482 (1994); **74**, 3088 (1995).
- ²²B.A. Jones and C.B. Hanna, *Phys. Rev. Lett.* **72**, 4253 (1994).
- ²³P. Bruno, *J. Magn. Magn. Mater.* **121**, 248 (1993); *Europhys. Lett.* **23**, 615 (1993).
- ²⁴M. Villeret, *J. Magn. Magn. Mater.* (to be published).
- ²⁵M.C. Muñoz and J.L. Pérez-Díaz, *J. Magn. Magn. Mater.* (to be published).
- ²⁶J.L. Pérez-Díaz, Ph.D. thesis, Universidad Complutense de Madrid, 1994.
- ²⁷A. Beckmann, M. Klaua, and K. Meinel, *Phys. Rev. B* **48**, 1844 (1993).
- ²⁸W. Jackolski, V.R. Velasco, and F.J. García-Moliner, *Phys. Scr.* **43**, 337 (1991).
- ²⁹M.C. Muñoz, V.R. Velasco, and F.J. García-Moliner, *Phys. Scr.* **35**, 504 (1987).
- ³⁰M.C. Muñoz, V.R. Velasco, and F. García-Moliner, *Phys. Rev. B* **39**, 1786 (1989).
- ³¹F. García-Moliner and V.R. Velasco, *Theory of Single and Multiple Interfaces* (World Scientific, Singapore, 1992).
- ³²D.A. Papaconstantopoulos, *Handbook of the Band Structure of Elemental Solids* (Plenum Press, New York, 1986).
- ³³V.L. Moruzzi, J.F. Janak, and A.R. Williams, *Calculated Electronic Properties of Metals* (Pergamon, New York, 1978).
- ³⁴C.M. Schneider, P. Schuster, M. Hammond, H. Ebert, J. Noffke, and J. Kirschner, *J. Phys. C* **3**, 4349 (1991).
- ³⁵J.L. Pérez-Díaz and M.C. Muñoz, *Phys. Rev. B* **50**, 8824 (1994).
- ³⁶M.G. Samant, J. Stöhr, S.S.P. Parkin, G.A. Held, B.D. Hermsmeier, F. Herman, M. van Schilfhaarde, L.-C. Duda, D.C. Mancini, N. Wassdahl, and R. Nakajima, *Phys. Rev. Lett.* **72**, 1112 (1994).